Afyon Kocatepe Üniversitesi Fen ve Mühendislik Bilimleri Dergisi
Afyon Kocatepe University – Journal of Science and Engineering
https://dergipark.org.tr/tr/pub/akufemubid

Araştırma Makalesi / Research Article
e-ISSN: 2149-3367
DOI: https://doi.org/10.35414/akufemubid.1694266
CITE: Afyon Kocatepe University Journal of Science and Engineering 26(2) (2026) 421-430

Investigation of The Effect of W Addition to FeB Hard Surface Alloy

*Makale Bilgisi / Article Info
Alındı/Received: 15.05.2025
Kabul/Accepted: 28.10.2025
Yayımlandı/Published: 08.04.2026

FeB Esaslı Sert Yüzey Alaşımına W İlavesinin Etkisinin İncelenmesi

Orhan AKYILDIZ[1*], Mustafa DURMAZ[2], Bülent KILINÇ[3], Şaduman ŞEN[2], Uğur ŞEN[2]

[1] *Sakarya Üniversitesi, Fen Bilimleri Enstitüsü, Metalurji ve Malzeme Mühendisliği Bölümü, Sakarya, Türkiye*
[2] *Sakarya Üniversitesi, Mühendislik Fakültesi, Metalurji ve Malzeme Mühendisliği Bölümü, Sakarya, Türkiye*
[3] *Sakarya Uygulamalı Bilimler Üniversitesi, Arifiye Meslek Yüksekokulu, Makine ve Metal Teknolojileri Bölümü, Sakarya, Türkiye*

Abstract

In this study, the effect of W addition to Fe-B based hard surfacing filler alloy was investigated. For this purpose, electric arc welding electrode was produced by adding 5% and 10% W to $Fe_{17}B_3$ hard surfacing filler compound and hard surfacing alloy was applied by welding on AISI 1010 steel substrate plate. After the welding process, it was observed that hard boride phases were formed in situ in the microstructure. As a result of XRD analysis, α-Fe and Fe_2B phases were detected in Fe-B based coating. It was determined that FeWB phase was also present together with α-Fe and Fe_2B phase in Fe-W-B based coatings. As a result of hardness measurements, micro hardness of Fe-B based composition was determined as 303-341 HV while surface hardness was 28 HRC. When 5% and 10% W element was added to the coating compound, hardness values increased and micro hardness values of 470-699 HV and 642-756 HV were reached, respectively. SEM images showed that the wear microstructures were adhesive, abrasive, fatigue and oxidative in character. The friction coefficient values obtained from the wear tests of the coatings were determined to be between 0.55-0.8. Wear rates were measured between $0.8x10^{-5}$ - $1.15x10^{-5}$ mm^3/m.

Keywords: *Hardfacing; Electric arc; Boride; Hardness; Wear*

Öz

Bu çalışmada Fe-B esaslı sert yüzey dolgu alaşımına W ilavesinin etkisi incelenmiştir. Bu amaçla $Fe_{17}B_3$ sert yüzey dolgu bileşiğine %5 ve %10 W eklenerek elektrik ark kaynak elektrodu üretilmiş ve AISI 1010 çelik altlık plaka üzerine sert yüzey alaşımı kaynak yapılarak uygulanmıştır. Kaynak işleminden sonra mikro yapıda in-situ olarak sert borür fazlarının oluştuğu gözlenmiştir. XRD analizleri sonucunda, Fe-B esaslı kaplamada α-Fe ve Fe_2B fazları tespit edilmiştir. Fe-W-B esaslı kaplamalarda ise α-Fe ve Fe_2B fazı ile birlikte FeWB fazının da bulunduğu belirlenmiştir. Sertlik ölçümleri sonucunda, Fe-B esaslı bileşimin mikro sertliği 303-341 HV arasında iken yüzey sertliği 28 HRC olarak tespit edilmiştir. Kaplama bileşimine %5 ve %10 W elementi eklendiğinde ise sertlik değerleri artarak sırasıyla 470-699 HV ve 642-756 HV mikro sertlik değerlerine ulaşılmıştır. SEM görüntüleri aşınma mikroyapılarının adhezif, abrazif, yorulma ve oksidatif karakterde olduğunu göstermiştir. Kaplamaların aşınma testleri sonucu elde edilen sürtünme katsayı değerleri 0,55-0,8 arasında tespit edilmiştir. Aşınma oranları ise $0,8x10^{-5}$-$1,15x10^{-5}$ mm^3/m arasında ölçülmüştür.

Anahtar Kelimeler: *Sert yüzey kaplama; Elektrik ark; Borür; Sertlik; Aşınma*

1. Introduction

Hardfacing is a surface coating method applied using different welding methods to obtain a special alloy surface layer on the surfaces of metal parts to increase the resistance of metal materials to wear or to restore the dimensions of the parts to their original size. Hardfacing provides economic benefits such as extending the working life of metal parts, reducing the need for part replacement, reducing maintenance time, producing the main part from cheap materials, reducing disassembly and assembly time and reducing overall costs. Hardfacing alloys come in a wide variety required for all metal materials. Some alloys were developed to form a hardfacing layer, others to restore parts to their original dimensions (CAVCAR, n.d.).

Hard surface coating is applied by a wide variety of methods. These methods include submerged arc welding (SAW) (Singh & Singh, 2019), flux cored wire arc welding (FCAW) (Sá de Sousa et al., 2021), MIG-MAG welding (GMAW) (Amushahi et al., 2010), plasma transfer arc welding (PTAW) (G.P. et al., 2019), gas tungsten arc welding (GTAW) (Zikin et al., 2013) and shielded metal arc welding (SMAW) (Baghel, 2022). Among these methods, the addition of alloys to the weld pool in the electric arc welding process with a covered electrode is relatively easy as it is done by means of ferro-alloys in the electrode cover. The low dilution between the cladding layer and the base material is the reason why ferroalloys are preferred (P, Manuel Rodriguez, 2007). Surface alloying of steels is a process in which, by the addition of alloy of a desired composition, a thin surface layer of alloy powder

*Sorumlu Yazar/Corresponding Author: Orhan AKYILDIZ e-posta/e-mail: orhan.akyildiz4@ogr.sakarya.edu.tr

and substrate material is simultaneously melted and rapidly solidified to form a dense coating metallurgically bonded to the substrate (Hojjatzadeh et al., 2012).

Borides are hard phases commonly used in hardfacing coatings. Borides obtained with transition metals have high hardness, wear, friction and corrosion resistance (Karip et al., 2015; Yoo et al., 2006). In today's world where wear and corrosion resistance is important, Fe-B alloys have gained importance due to their excellent wear and corrosion resistance. (Ingole et al., 2005; Zhang et al., 2019). The Fe-W-B system has attracted increasing interest in recent years in response to the need for hard and wear-resistant materials. FeWB is gaining importance due to its properties such as high hardness, high melting point, excellent chemical stability and very good wear resistance at high temperature (Li et al., 2017).

In the literature, there are many studies in which metal addition is made to Fe-B based hard surface alloy. For example, Zhuang et al. investigated the effect of Mn and V addition to Fe-B hard surface alloy on microstructure and wear behavior. The addition of Mn and V increased the hardness and wear resistance of the surface alloy layer and improved its performance. It was found that the sample with 20.15% Mn and 4.69% V content exhibited optimum performance (Zhuang et al., 2024). Yüksel et al. observed that carbides increased with increasing FeB content in their study using flux cored wire welding method. The increase in carbides also increased the hardness. Both the wire/powder mixture ratio and the FeB content in the powder mixture affected the wear resistance. Wear loss decreased with the increase of FeB in the powder mixture (Yüksel, 2014). Abakay et al. showed that surface alloying with Fe-W and Fe-B can be developed effectively and economically by TIG welding on AISI 1020 steel. They found that the surface alloyed layer with Fe-W and Fe-B on plain carbon steel has a eutectic microstructure of FeB and FeW_2B_2 phases as in-situ composite structure and the phases formed in the alloyed layers are Fe_2B, FeB and FeW_2B_2 as main phases, W_2B and W_2B_5 as trace phases (Abakay et al., 2014). In another study, they produced 50%Fe-10%W-40%B (atomic) alloy system using TIG welding method. And they investigated the friction and wear properties of this alloy system (Abakay et al., 2015). Additionally, there are many studies in the literature on hardfacing coating using the coated electrode welding method. Kocaman et al. produced Fe-M (Cr, Ti, Mo)-B based hardfacing coatings by adding various ferroalloys to the electrode coating. They investigated the microstructure and mechanical properties of the coatings (Kocaman, 2023, Kocaman et al., 2021, Kocaman et al., 2022a, Kocaman et al., 2022b). Recep et al. produced $Fe_{(15-x)}MoTiB_xMn_2C$(x=0, 1, 2, 3)-based hardfacing coatings by adding ferro-molybdenum, ferro-manganese, ferro-titanium, and ferro-boron to the electrode coating. They investigated the effects of boron on the microstructure and wear in these coatings. (Recep et al., 2024).

Although there are few studies in which Fe-B-W alloy system is applied by electric arc welding method, in this study, Fe-B based hardfacing alloying electrodes were produced and the effect of W addition to these hard surface alloying electrodes was investigated. The produced electrodes were hard surface alloyed on the substrate material using electric arc welding method. Microstructure and phase analysis, hardness and wear tests were carried out by taking samples from the required parts of the hard surface alloy welding coatings. Microstructures were analyzed by SEM, EDS and XRD methods. The hardness of the hardfacing alloys was measured using a Vickers hardness tester for microhardness values. Macro hardness values were also measured by Rockwell hardness tester. Finally, the wear properties of hardfacing alloys were investigated.

2. Materials and Methods

In this study, the covered hardfacing electrode, whose chemical composition is given in Table 1, was produced, and coated on the surface of the steel substrate using the electric arc welding method. Ferro alloy powders supplied from Aveks and ARMCO companies. with chemical composition given in Table 2 were used for the electrode cover.

Table 1. Chemical composition of electrode (at. %)

Composition	W	B	Fe
$Fe_{17}B_3$	-	15	85
$Fe_{16}WB_3$	5	15	80
$Fe_{15}W_2B_3$	10	15	75

Table 2. Chemical composition of ferroalloy powders (wt. %)

Ferro-alloys	W	B	C	Mn	Fe
Ferrous-tungsten	77.98	-	0.11	0.057	Bal.
Ferrous-boron	-	18.58	0.31	0.065	Bal.
Iron powder	-	-	-	-	99.9

Table 3. Chemical composition of core metal (wt. %)

Core metal	C	Cr	Mn	Si	P	S	Fe
H08A	<0.1	0.064	0.37	0.1	<0.02	<0.02	Bal.

H08A low carbon steel rod, whose chemical composition is given in Table 3, was used as the core metal. During the welding process, flux (TiO_2, CaF_2, $CaCO_3$, SiO_2, Al_2O_3, potassium alginate and potassium titanate) materials were added to the cover at the rate of 5 wt% for the electrode to fulfill its function. In addition, 20% by weight of potassium silicate ($K_2O.SiO_2$) was added to the cover

composition in order for the powders used in electrode production to adhere to the core metal surface.

Ferro alloys supplied as rocks from the companies were ground in a ring mill with a sieve size below 100 µm. Then, the amount of powder to be weighed was determined within the framework of the program specially prepared for electrode composition calculation and powder weighing processes were carried out. The weighed powders were first subjected to dry mixing and then wet mixing to obtain a viscous slurry. The viscous slurry obtained was taken into the mold with a diameter of 5.5 mm, which was specially prepared for electrode production, and then the core rod with a diameter of 2.5 mm was passed through the viscous slurry in the mold. The final electrodes were kept at room temperature for 24 hours. Then they were kept at 350 °C for 2.5 hours to complete the production and made ready for welding.

The electrodes produced within the scope of the study were coated on AISI 1010 steel substrates whose chemical composition is given in Table 4 and measured as 70x30x8 mm. Coating processes were carried out with Magmaweld RD 650 E electric arc welding machine with 125 A welding current, 25V welding voltage, 0.3 m/min welding speed with direct current reverse polarity. The process steps are shown in the diagram below:

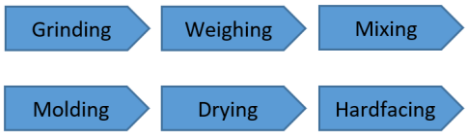

Table 4. Chemical composition of base metal

Substrate	C	Mn	Si	P	S	Fe
AISI 1010	0.09	0.4	0.024	0.026	0.022	Bal.

After coating, the specimens were cut to the appropriate dimensions for the investigations, sanded to 1200 grit SiC sandpaper and polished with 0.3 µm alumina paste. The samples to be used for microstructure investigations were etched with 3% Nital solution. Microstructure examinations were carried out with a JEOL JSM-6060 LV scanning electron microscope (SEM). Point and localized elemental analysis was carried out with IXRF System INC. energy dispersive spectroscopy (EDS) integrated into the SEM. RIGAKU D/MAX/2200/PC x-ray diffractometer (XRD) (CuKα λ=1,5408 Ao) was used for phase analysis. FutureTech FM700 microhardness tester was used to determine the in-line hardness values of the coating. Row hardness tests were measured in Vickers (Hv0.3) at 0.2 mm intervals from the substrate. The hard surface coating layer was subjected to abrasion tests parallel to the substrate surface. Wear tests were performed with TRIBOtechnic-TRIBOtester tester according to ASTM G133 standard. Wear tests were carried out at 25^{0}C (±2) room temperature and 30% (±3) humidity conditions. A 10 mm diameter Al_2O_3 (1850 $HV_{0.1}$) ball was used in the tests. The tests were carried out under three different loads of 2N, 4N and 8N, at a distance of 100 m, at a speed of 30 mm/sec and a range of motion 5 mm. After the tests were performed, the test traces were measured with a TaylorHobson 2D surface profilometer to verify the test results. The volume of traces produced in the tests was calculated according to the formula given in Eq1. Wear rate values are determined in equation 2.

$$V=Axl \quad (1)$$

In the formula; V: track volume (mm^3), A: track cross-sectional area (mm^2), l: track length (mm).

$$W = \frac{V}{Total\ Distance} \quad (2)$$

In the formula; W: represents the wear rate.

3. Results and Discussions

3.1. Microstructure

Figure 1 shows the SEM images of the coating interface and the coating layer of the single pass hard surface alloyed samples with $Fe_{(17-x)}W_xB_3$ composite electrode. It can be seen that the hardfacing layers exhibit a metallurgical bond with the substrate. For each sample, three distinct regions consisting of the plating layer, the interface and the substrate can be clearly distinguished. It was also determined that the coating layers have a smooth surface without porosity.

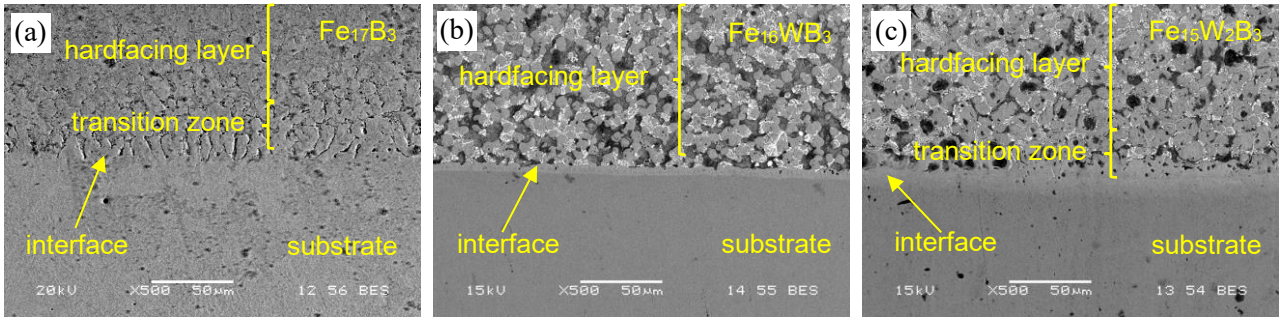

Figure 1. (a) $Fe_{17}B_3$ alloy interface (b) $Fe_{16}WB_3$ alloy interface (c) $Fe_{15}W_2B_2$ interface

Figure 2 shows the XRD patterns of $Fe_{17}B_3$, $Fe_{16}WB_3$ and $Fe_{15}W_2B_3$ hard surface alloys. α-Fe and Fe_2B phases were detected in Fe-B based hardfacing. In Fe-W-B based coatings, in addition to α-Fe and Fe_2B phases, FeWB phase was also detected. These phases were found to be compatible with the Fe-W-B ternary equilibrium diagram (Raghavan, 1992).

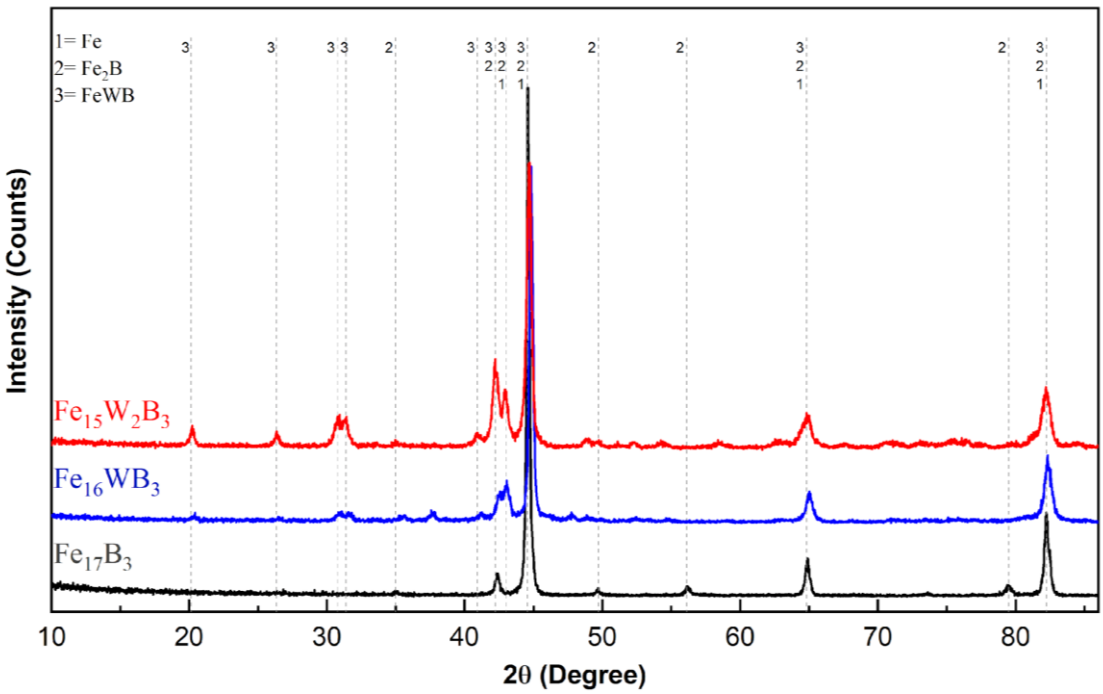

Figure 2. XRD patterns of $Fe_{(17-x)}W_xB_3$ based

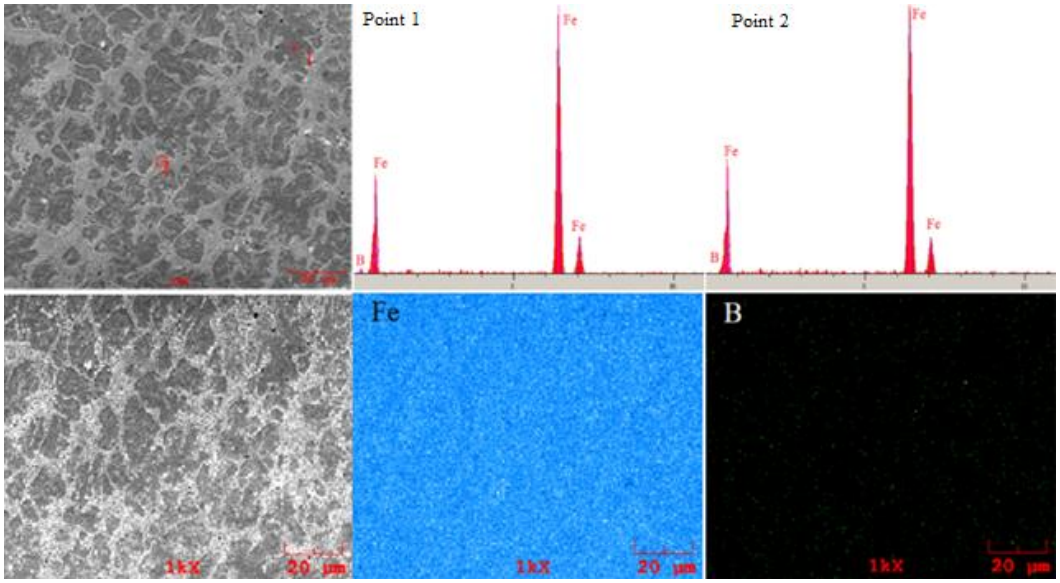

Figure 3. SEM, EDS and MAP analysis of $Fe_{17}B_3$ based hardfacing alloy

SEM images, EDS and MAP analysis of Fe-W-B based hardfacing alloys are given in Figures 3-5. When the microstructure of the $Fe_{17}B_3$ based coating with an atomic B ratio of 15% and no W in its structure is examined, two different regions are clearly seen. This composition has a hypoeutectic microstructure. The dark gray regions are the primary phase and the light-colored regions are composed of eutectic phases. When the EDS analysis number 1 in Figure 3 and the MAP analysis are examined, it is seen that the dark gray region is intensely composed of Fe element. Considering the X-ray analysis given in Figure 2, it is determined that this region is α-Fe. Again, when the EDS analysis number 2 taken from the eutectic region in Figure 3 is examined, there is a qualitative presence of B element together with Fe element. According to MAP and XRD analyses, this eutectic structure contains of α-Fe+Fe_2B phases.

Figure 4 shows the SEM, EDS and MAP analysis of $Fe_{16}WB_3$ based coating. SEM images show a microstructure consisting of dark gray, eutectic and white regions. In the EDS and MAP analysis number 1 taken from the white region, Fe and B are seen together with W intensely. In XRD analysis, FeWB phase was detected in W-containing coatings and it was comprehend that the white region consisted of this phase. When we examined the EDS analysis number 2 of the dark gray region, Fe and W were identified. Here it is seen that Fe concentration is high. Hence, it is thought that this region is formed from the α-Fe phase. When the number 3 and 4 EDS analyses taken from the eutectic region were inspected, Fe, B and partly W elements were identified. When the Fe_2B phase detected in XRD is taken into consideration, it is understood that this eutectic structure is formed from α-Fe+Fe_2B.

When the SEM images of the $Fe_{15}W_2B_3$ coating are examined in Figure 5, it is observed that the microstructure contains of two regions. In EDS analysis numbered 1 and 3 taken from the white eutectic structure, W, Fe, B and C were detected and it was characterized that this structure consists of α-Fe+FeWB phase. Fe element is present densely in EDS analysis number 2 taken from the dark region. Hence, This region is thought to consist of α-Fe.

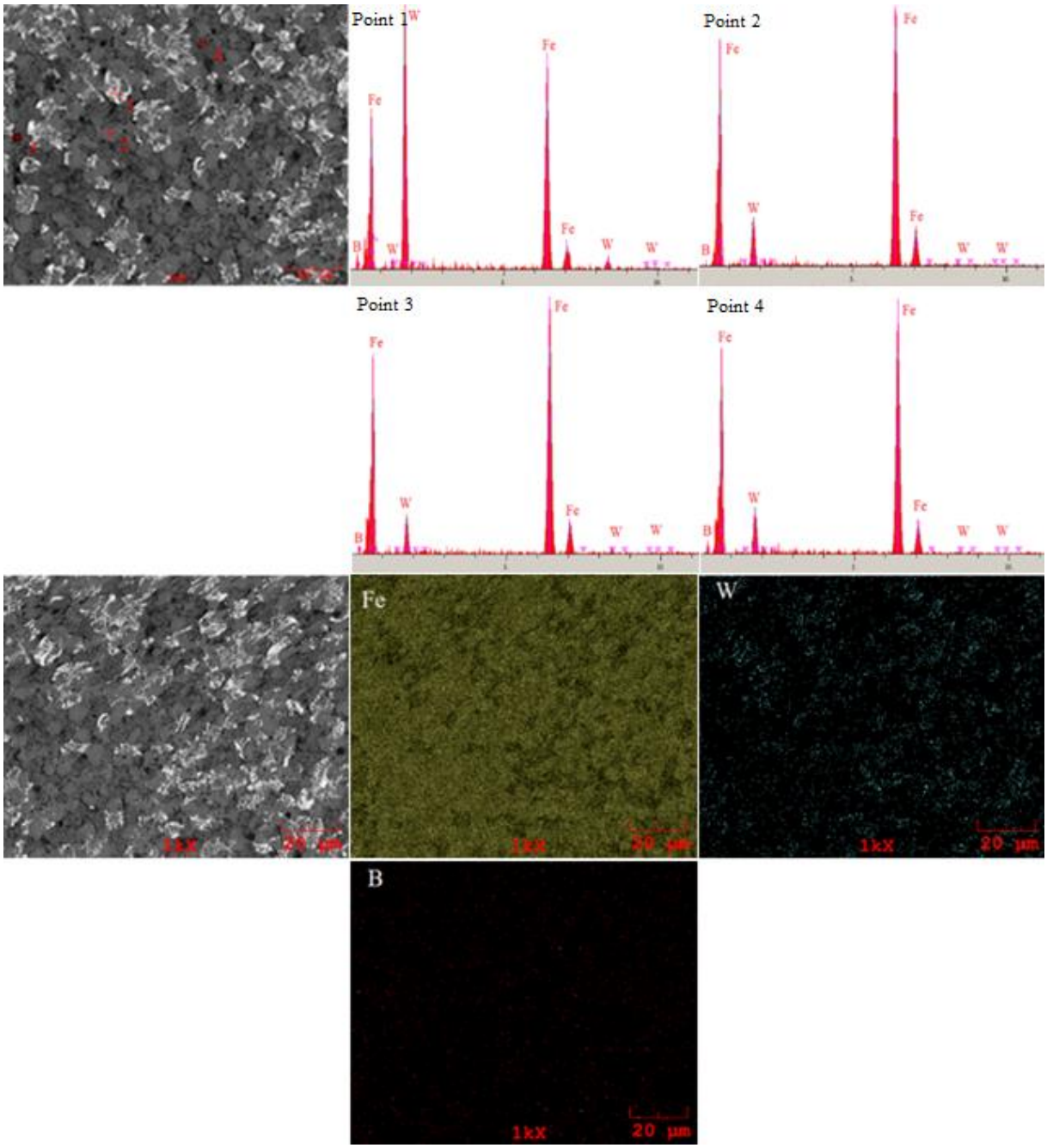

Figure 4. SEM, EDS and MAP analysis of $Fe_{16}WB_3$ based hardfacing alloy

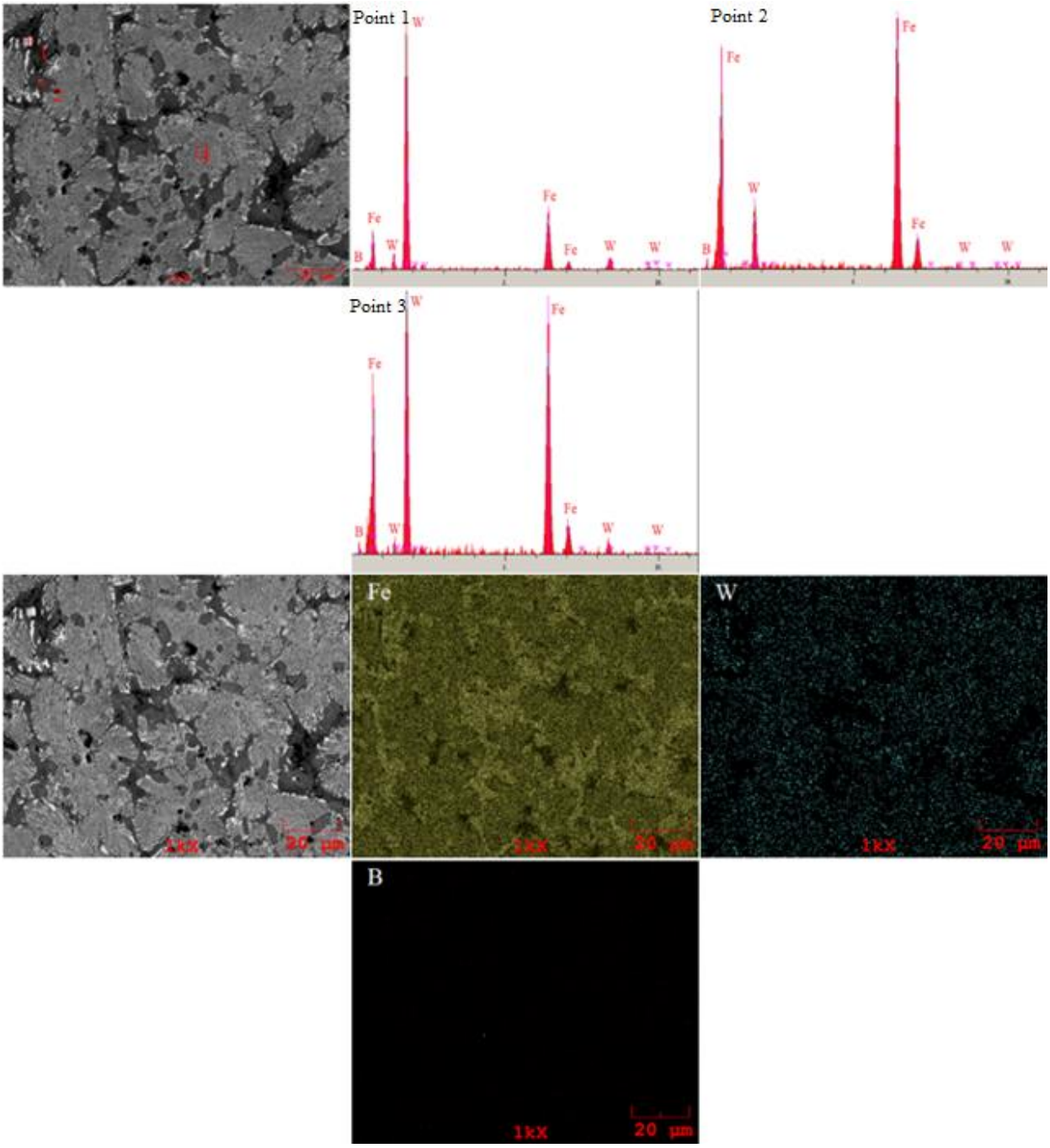

Figure 5. SEM, EDS and MAP analysis of $Fe_{15}W_2B_3$ based hardfacing alloy

3.2. Hardness

Figure 6 and 7 shows the row hardness and surface hardness values of $Fe_{(17-x)}W_xB_3$ based hard surface coatings. The microhardness of the Fe-B based composition was measured between 303-341 HV. The surface hardness of this coating layer was measured as 28 HRC. The microhardness values of the coating layer containing 5% and 10% W were found to be between 470-699 HV and 642-756 HV, respectively.

Considering the Fe-B based composition, as a result of the sequence hardness tests, the microhardness values of the coating layers increased pronouncedly with the addition of 5% and 10% W In this system.

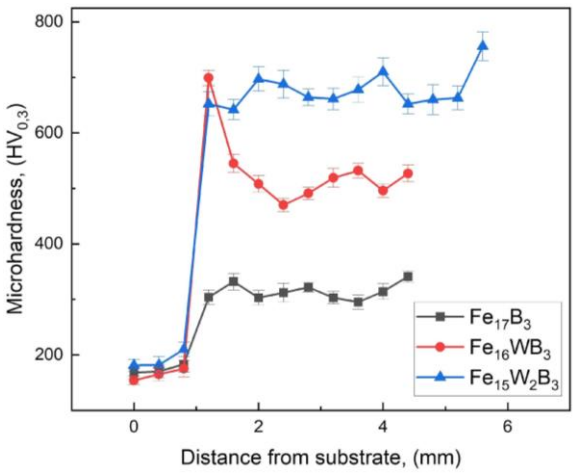

Figure 6. Microhardness values of hardfacing alloy

With increasing W addition, the proportion of eutectic structures in the coating microstructure increased and accordingly the hardness value increased significantly (Durmuş et al., 2018).

When the macro hardness values of Fe-W-B based hard surface alloying containing 5% and 10% W were examined, they were measured as 32 and 43 HRC, respectively, and in this test, the highest HRC hardness value was measured in the coating with 10% W ratio.

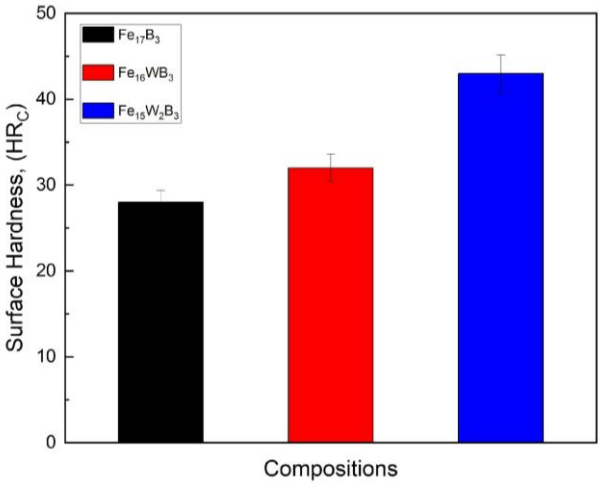

Figure 7. Macro hardness values of hardfacing alloy

3.3. Wear

Figure 8 shows the elements determined as a result of SEM images and EDS analysis of the worn surfaces of $Fe_{17}B_3$, $Fe_{16}WB_3$, $Fe_{15}W_2B_3$ hard surface alloyed samples under 2N and 8N load.

When the SEM images taken from the wear traces of $Fe_{17}B_3$ hard surface alloy with an average microhardness of 314 HV are examined, it is seen that there is mostly abrasive wear on the surface of our sample under 2N load and partially adhesive wear mechanism (Figure 8. (a and b)). As the load increases (2N, 8N), it is seen that there is increasing adhesive wear instead of decreasing abrasive wear. In addition, microcracks were observed on the worn surface under 2N load. When the EDS analysis obtained from SEM images is examined, the presence of iron and aluminum elements as well as oxygen elements on the wear surfaces is observed. In this case, it is possible to talk about the oxidative wear mechanism together with the abrasive, adhesive wear mechanism on the worn surface of the $Fe_{17}B_3$ sample.

When we examine the SEM images of the worn surfaces of the $Fe_{16}WB_3$ hard surface alloy obtained by adding 5% W to $Fe_{17}B_3$ alloy in Figure 8. (c and d), the adhesive wear on the wear surface increased and abrasive wear decreased significantly with the increase in the hardness of 5% W (average 531 HV). The intensity of adhesive wear increased with increasing the load. Again in this sample, EDS analysis obtained from SEM images shows that there is an oxidative wear mechanism in places.

When we examine the SEM images of the $Fe_{15}W_2B_3$ hard surface alloy obtained by adding 10% W to $Fe_{17}B_3$ alloy in Figure 8 (e and f), abrasive scratches are observed at 2N load, but their severity is less than the other samples, with the addition of 10% tungsten further increasing the hardness (average 676 HV). It is possible to say that the increase in the volume fraction of eutectic structures consisting of borides, especially in the microstructure, acts as a barrier during wear. In this case, the severity of abrasive wear decreased. At 8N load, it is seen that the abrasive scratches are slightly deeper. Cracks were also observed on the abraded surfaces. Again, as in the other samples, oxygen was detected on the worn surfaces as a result of EDS analysis. It is possible to talk about abrasive, adhesive, oxidative wear mechanism as well as fatigue wear in this sample.

Figure 9 shows the coefficient of friction values of $Fe_{17}B_3$, $Fe_{16}WB_3$, $Fe_{15}W_2B_3$ hard surface alloys. When the graph is examined, the coefficient of friction ratios decreased with the increase in the load applied during the wear test for $Fe_{17}B_3$ composition. In $Fe_{16}WB_3$ and $Fe_{15}W_2B_3$ compositions, the coefficient of friction ratios increased slightly by increasing the load applied during wear from 2N to 4N, but this ratio decreased significantly during wear under 8N load. The decrease in friction coefficients with increasing wear load can be attributed to the lubricating effect of oxide products formed on the worn surface (Kocaman et al., 2021). In addition, it was observed that the friction coefficient of W-added $Fe_{16}WB_3$ and $Fe_{15}W_2B_3$ compositions was lower than $Fe_{17}B_3$ at 2N and 4N loads. The opposite is the case at 8N load.

Figure 10 shows the wear rates of $Fe_{17}B_3$, $Fe_{16}WB_3$, $Fe_{15}W_2B_3$ hardfacing coatings. It is clearly observed from the graph that the increasing W ratio in the coating system has a decisive effect on the decrease in the wear rate. For all loads, the wear rate decreased with increasing W ratio. The reason for this situation can be considered as the increase in the eutectic hard boride structure (α-Fe+FeWB) ratios in the microstructure with increasing W and accordingly the hardness of the coatings increases. It is also observed from the graph that the wear rates of the coatings increase with increasing wear load.

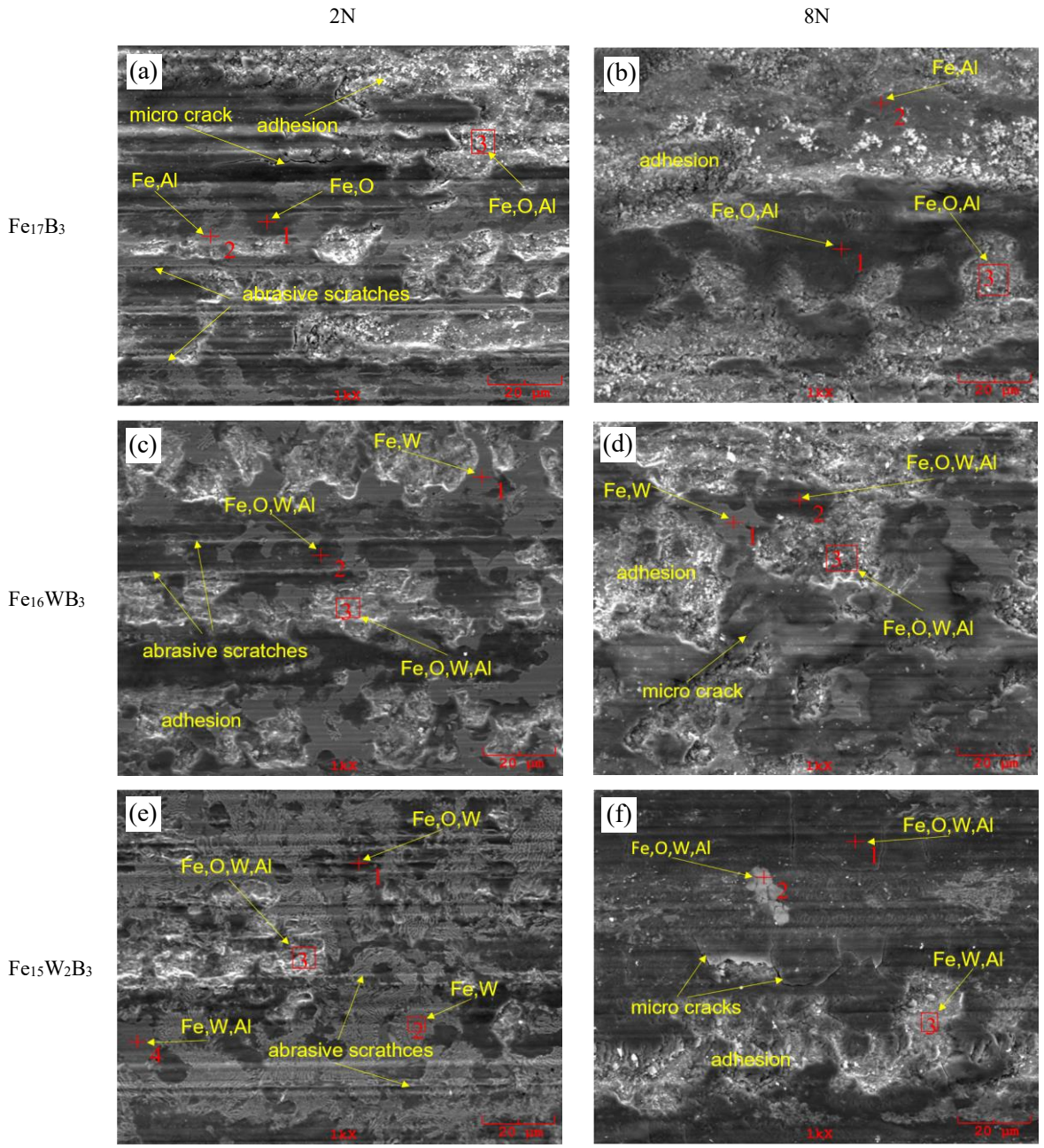

Figure 8. SEM images and EDS analyze of worn surfaces of hardfacings under 2N and 8N test loads

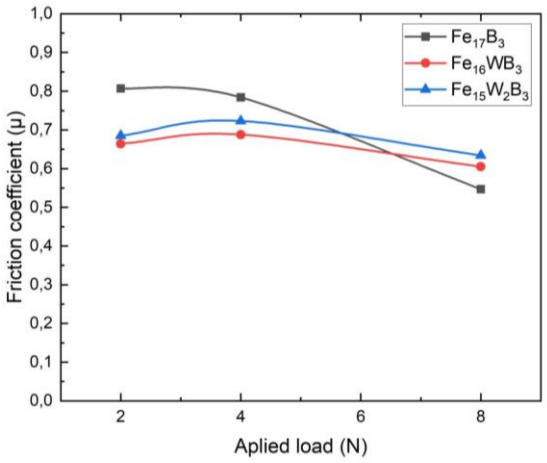

Figure 9. Friction coefficient values of hardfacing alloys under 2N, 4N, 8N load

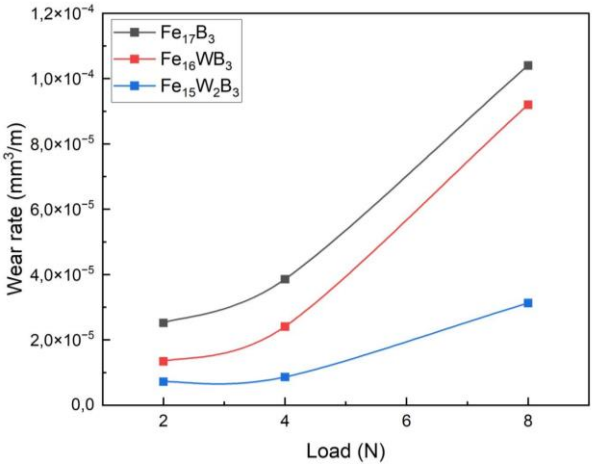

Figure 10. Wear rates of hardfacing alloys under 2N, 4N, 8N load

4. Conclusions

The hard surface alloy layer with Fe-W-B composition was successfully formed on the surface of AISI 1010 base steel by electric arc welding method. Three different layers consisting of hardfacing layer, transition zone and interfacial surface were identified, and it was observed that the coating layer formed a metallurgical bond with the substrate. As a result of XRD analysis, α-Fe and Fe_2B phases were detected in Fe-B based coating; FeWB phase was also detected in Fe-W-B based coatings in addition to α-Fe and Fe_2B phases. The coating layer of $Fe_{17}B_3$ composition was found to have a sub-eutectic microstructure consisting of primary α-Fe and α-Fe+Fe_2B (eutectic) phases. The $Fe1_6WB_3$ composition shows a microstructure with dark gray, eutectic and white regions. The dark gray region is α-Fe, the eutectic structure is α-Fe+Fe_2B and the white regions are FeWB phases. The microstructure of the $Fe_{15}W_2B_3$ coating was observed to consist of two regions. It was determined that the white colored eutectic structure consists of α-Fe + FeWB phase and the dark region consists of α-Fe. With the addition of 5% W to the $Fe_{17}B_3$ composition, the micro hardness value increased from 314 HV to 531 HV, and the macro hardness increased from 28 HRC to 32 HRC. With the addition of 10% W, the micro hardness was 676 HV and the macro hardness was 43 HRC. When we examined the wear tests of the hard surface coatings, it was observed that the wear rate increased with the increase of the load under 2N, 4N and 8N loads. In addition, the wear rate decreased with the increase of W ratio for all loads. Abrasive, adhesive, fatigue wear and oxidative wear mechanisms were detected on the worn surfaces.

Declaration of Ethical Standards

The authors declare that they comply with all ethical standards.

This study is derived from master thesis (thesis number: 841745) under the supervision of Prof. Dr. Uğur Şen by 2023 on date of Investigation of the effect of added W, Nb and Cr on the properties of Fe-B based hard filler electrode alloy Titled.

Credit Authorship Contribution Statement

Author-1: Conceptualization, investigation, methodology and software, visualization and writing – original draft.
Author-2: Conceptualization, investigation, methodology and software, supervision and writing – review and editing.
Author-3: Conceptualization, investigation, methodology and software, supervision and writing – review and editing.
Author-4: Conceptualization, investigation, methodology and software, supervision and writing – review and editing.
Author-5: Conceptualization, investigation, methodology and software, supervision and writing – review and editing.

Declaration of Competing Interest

The authors have no conflicts of interest to declare regarding the content of this article.

Data Availability Statement

All data generated or analyzed during this study are included in this published article.

5. References

Abakay, E., Kilinc, B., Sen, S., & Sen, U. (2014). *Microstructural Examinations of Fe-W-B Base Hard-Faced Steel*. https://doi.org/10.1007/978-3-319-04639-6

Abakay, E., Kilinc, B., Sen, S., & Sen, U. (2015). *Wear Properties of TIG Surface Alloyed Steel with 50 % Fe-10 % W-40 % B Alloy*. *127*(4), 957–960. https://doi.org/10.12693/APhysPolA.127.957

Amushahi, M. H., Ashrafizadeh, F., & Shamanian, M. (2010). Characterization of boride-rich hardfacing on carbon steel by arc spray and GMAW processes. *Surface and Coatings Technology*, *204*(16–17), 2723–2728. https://doi.org/10.1016/j.surfcoat.2010.02.028

Baghel, P. K. (2022). Effect of SMAW process parameters on similar and dissimilar metal welds : An overview. *Heliyon*, *8*(June), e12161. https://doi.org/10.1016/j.heliyon.2022.e12161

Cavcar, M. M. (n.d.). *SERT DOLGU ALAŞIMLARI*. Oerlicon Kaynak Elektrodları Ve Sanayi A.Ş.

Durmuş, H., Çömez, N., Gül, C., Yurddaşkal, M., & Yurddaşkal, M. (2018). Wear performance of Fe-Cr-C-B hardfacing coatings: Dry sand/rubber wheel test and ball-on-disc test. *International Journal of Refractory Metals and Hard Materials*, *77*, 37–43. https://doi.org/10.1016/j.ijrmhm.2018.07.006

Hojjatzadeh, S. M. H., Halvaee, A., & Sohi, M. H. (2012). Surface alloying of AISI 1045 steel in a nitrogen environment using a gas tungsten arc process. *Journal of Materials Processing Technology*, *212*(11), 2496–2504. https://doi.org/10.1016/j.jmatprotec.2012.06.006

Ingole, S., Liang, H., Usta, M., Bindal, C., & Ucisik, A. H. (2005). *Multi-scale wear of a boride coating on tungsten*. *259*, 849–860. https://doi.org/10.1016/j.wear.2004.12.024

Karip, E., Aydin, S., & Muratoɫlu, M. (2015). A study on hardfacing alloy using Fe-Cr and Fe-B Powders. *Acta Physica Polonica A*, *128*(2), 160–163. https://doi.org/10.12693/APhysPolA.128.B-160

Kocaman, E. (2023). Effect of the Molybdenum Content on Wear and Corrosion Behavior of Fe-B-Based Surface-Alloyed Layer. *Coatings*, *13*(12). https://doi.org/10.3390/coatings13122050

Kocaman, E., Kılınç, B., Şen, Ş., & Şen, U. (2021). *Effect of chromium content on Fe(18-x)CrxB2(X=3,4,5) hardfacing electrode on microstructure , abrasion and corrosion behavior Effect of chromium content on $Fe_{(18-x)}Cr_xB_2$ (X=3, 4, 5) hardfacing electrode on*. *1*, 177–190. https://doi.org/10.17341/gazimmfd.689230

Kocaman, E., Kılınç, B., Şen, Ş., & Şen, U. (2022a).

Development of Surface Properties with In Situ TiB2 Intermetallic-Assisted Coating by Fe(18-X)Ti2BX (x = 3,4,5)-Based Electrodes. *Arabian Journal for Science and Engineering*, *47*(7), 8485–8501. https://doi.org/10.1007/s13369-021-06304-0

Kocaman, E., Kılınç, B., Şen, Ş., & Şen, U. (2022b). In-situ TiB2 and Fe2Ti intermetallic assisted hard coatings by Fe-Ti-B based hardfacing electrodes. *Journal of Alloys and Compounds*, *900*. https://doi.org/10.1016/j.jallcom.2021.163478

Li, C., Yang, G., Liu, Y., Qiu, Y., & Li, J. (2017). A novel route of synthesising Fe–W–B alloy powders and characterisation thereof. *Powder Metallurgy*, *60*(4), 241–248. https://doi.org/10.1080/00325899.2016.1266812

P, Manuel Rodriguez, C. C. A. (2007). *Operational behavior assesment of coated tubular electrodes for SMAW hardfacing Amado Cruz Crespo a , Am ´. 9*, 265–273. https://doi.org/10.1016/j.jmatprotec.2007.07.048

Raghavan, V. (1992). *Phase Diagrams of Ternary Iron Alloys*. Indian Institute of Metals.

Rajeev. G.P., Kamaraj M., K., & Bakshi Sirinivasa. R. (2019). Comparison of microstructure, dilution and wear behavior of Stellite 21 hardfacing on H13 steel using cold metal transfer and plasma transferred arc welding processes. *Surface and Coatings Technology*, *375*(July), 383–394. https://doi.org/10.1016/j.surfcoat.2019.07.019

Recep, H., Engin, K., Bülent, K., Şaduman, Ş., & Uğur, E. N. (2024). Effect of Boron and Carbon on the Surface-Alloyed Layers with Fe(15−x)MoTiBxMn2C (x = 0,1,2,3)-Based Covered Electrodes. *Journal of Materials Engineering and Performance*, *33*(22), 12480–12493. https://doi.org/10.1007/s11665-023-08837-x

Sá de Sousa, J. M., Lobato, M. Q., Garcia, D. N., & Machado, P. C. (2021). Abrasion resistance of Fe–Cr–C coating deposited by FCAW welding process. *Wear*, *476*(September 2020), 203688. https://doi.org/10.1016/j.wear.2021.203688

Singh, A., & Singh, R. P. (2019). A review of effect of welding parameters on the mechanical properties of weld in submerged Arc welding process. *Materials Today: Proceedings*, *26*(2), 1714–1717. https://doi.org/10.1016/j.matpr.2020.02.361

Yoo, J. W., Lee, S. H., Yoon, C. S., & Kim, S. J. (2006). *The effect of boron on the wear behavior of iron-based hardfacing alloys for nuclear power plants valves*. *352*, 90–96. https://doi.org/10.1016/j.jnucmat.2006.02.071

Yüksel, N. (2014). *Wear behavior – hardness – microstructure relation of Fe – Cr – C and Fe – Cr – C – B based hardfacing alloys*. *58*, 491–498. https://doi.org/10.1016/j.matdes.2014.02.032

Zhang, J., Liu, J., Liao, H., Zeng, M., & Ma, S. (2019). A review on relationship between morphology of boride of Fe-B alloys and the wear / corrosion resistant properties and mechanisms. *Integrative Medicine Research*, *8*(6), 6308–6320. https://doi.org/10.1016/j.jmrt.2019.09.004

Zhuang, M., Liu, Q., Li, X., Ren, Y., Liu, X., Yan, Y., Yuan, S., Lv, P., & Ma, Z. (2024). *Effect of manganese and vanadium additions on the microstructures and two-body abrasive wear behaviors of Fe – B hardfacing alloys*. *169*(December 2023).

Zikin, A., Badisch, E., Hussainova, I., Tomastik, C., & Danninger, H. (2013). Characterisation of TiC – NiMo reinforced Ni-based hardfacing. *Surface & Coatings Technology*, *236*, 36–44. https://doi.org/10.1016/j.surfcoat.2013.02.027